JOURNAL OF MATERIALS SCIENCE 12 (1977) 1981–1987

Phase relationships in the system NiO-WO_3

L. WEBER, U. EGLI
Anorganisch-Chemisches Institut der Universität Zürich, Switzerland

The phase diagram of the system NiO–WO_3 was established by means of differential thermal analysis (DTA) supported by photoemission electron microscopy (PhEEM) and X-ray diffraction (XRD). The only compound, $NiWO_4$, melts incongruently (peritectic decomposition) at 1420° C and forms a eutectic with WO_3 at 73 mol % WO_3 and 1245° C. Primary phase crystallization as well as eutectic and peritectic solidification were studied by the comparison of the DTA measurements and the phase intergrowth morphologies as observed by PhEEM. The experimental liquidus lines are briefly discussed with reference to the calculated values.

1. Introduction

Tungstates of divalent metals, MWO_4, are known to crystallize in two major classes: alkaline-earth tungstates with M = Ca, Sr, Ba are described as scheelite type structures melting congruently at about 1500 to 1600° C; the corresponding quasi-binary phase systems MO–WO_3 have been studied in detail [1]; $MgWO_4$ and transition metal tungstates with M = Mn, Zn, Cd and the ferrous group with M = Fe, Co, Ni crystallize with wolframite structures. However, only the systems MgO–WO_3 [1] and CoO–WO_3 [2] have been investigated comprehensively. Both $MgWO_4$ and $CoWO_4$ melt congruently at 1358° C and 1280° C, respectively.

In the present work, the phase diagram of the system NiO–WO_3 was determined. The melting and crystallization behaviour of $NiWO_4$ and WO_3 were studied employing DTA mainly, X-ray diffraction (XRD) and photoemission electron microscopy (PhEEM). The latter method provides sensitive ceramographic informations on the phase intergrowth morphologies resulting from the solidification of the melts.

2. Experimental procedure

Reagent grade powder of black NiO and WO_3 were used as initial materials. The black NiO was heated for 3 h in air at 1200° C to obtain the green modification with stoichiometric composition [3]. NiO and WO_3 were then intimitely mixed in various molar portions corresponding to steps of 5% WO_3*.

* Chemical compositions are in mol % WO_3 throughout.

2.1. DTA

A conventional thermoanalyser (Mettler, Switzerland) with an upper temperature limit at 1600° C was used for the DTA measurements. Exactly weighted amounts of the powder mixtures (50 to 100 mg) were sealed in small platinum capsules (3 mm diameter and 18 to 20 mm length). As reference material, α-Al_2O_3 was used throughout. The temperature T of the reference and the temperature difference ΔT between reference and specimen were measured by means of Pt–Pt/10%Rh thermocouples. The temperature calibration (± 5° C) refers to the melting temperatures of gold at 1063° C [4] and of WO_3 at 1430° C [5], as well as to the known crystalline phase transition [6] of Mn_3O_4 at 1172° C.

Each particular sample was submitted to about 5 heating–cooling cycles to check the reproducibility of the results. Heating and cooling rates of 2, 6 and 10° C min^{-1} were applied for comparison. After the first melting process, the specimen material was situated in the lower part of the platinum capsule only, thus giving a good thermal contact with the thermocouple. Due to the arrangement of the thermocouple outside the sample, ΔT is independent on the thermal conductivity of the sample [7]. The onset of a chemical reaction is determined by graphical evaluation of the "extrapolated onset point" T_{eo} [8, 9] of the DTA peak. The end of the reaction is indicated by the peak maximum T_p [7, 8, 9]. While crossing a solid-liquid two-phase region with increasing

temperature, the solidus and liquidus temperatures are given by T_{eo} and T_p, respectively. The amount and radius of the sample were kept small to avoid peak distortion [10] and shifting of T_p.

Relative proportions of reaction enthalpies can be obtained by DTA peak area evaluations if the several samples are submitted to comparable experimental conditions [7, 10, 11]. This proportionality can be used for the exact determination of the eutectic composition [7, 8] as described below. The enthalpy of fusion of any compound can also be determined at least approximately by direct comparison with known standard materials.

The evaluation of each particular peak area was performed [8, 12] by separating it into two parts which are limited by the straight extensions of the "basic line" at each side of the peak and by a straight line perpendicular to the "time axis" at T_p, respectively (cf. Figs. 2, 9). This method has been proven to be more accurate and reliable [12] than other kinds of peak area evaluation [13].

2.2. PhEEM and XRD

Samples for the ceramographic examination by PhEEM had to be prepared in the following way: 1 to 2 g of powder mixtures were heated in platinum crucibles 7 mm in diameter for some minutes at about 1500° C. After melting was complete, the samples were either removed from the furnace to cool in air rapidly (mode A), or they were solidified in the furnace applying cooling rates of about 10 to 20° C min^{-1} (mode B). After this procedure, the solidified samples had the shape of a disk, and were ground and polished to get a smooth surface.

Details on the method of PhEEM and its application have been reported earlier [14, 15]. While porosity of the samples and relief structures on the surface are troubling factors for the investigation, PhEEM sensitively reflects even small chemical inhomogeneities (< 1%) of a sample. Since no surface etching was wanted prior to the investigation, phase boundaries and other small phase regions were preserved and could be examined. All samples were analysed at room temperature by X-ray diffraction (Guinier camera, Cu$K\alpha$ radiation).

3. Results

The phase diagram of the system NiO–WO_3 was obtained by the DTA measurements and is depicted in Fig. 1. The stable phase relations were determined by the melting temperatures of the heating runs (10° C min^{-1}), since no superheating of the melting solid phases was observed. The solidification temperatures of the cooling runs (10° C min^{-1}) indicated a characteristic supercooling of the melts prior to primary and eutectic crystallization. This is depicted in Fig. 1 by the metastable liquidus and solidus lines.

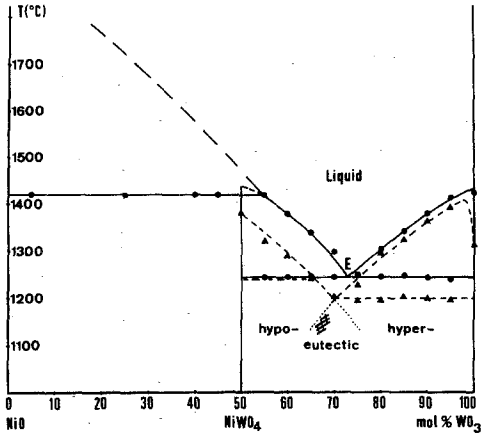

Figure 1 Phase diagram of the system NiO–WO_3. Solid lines and solid circles represent the stable phase relations as obtained by DTA heating runs (10° C min^{-1}). The dashed lines and solid triangles give the metastable phase relations as obtained by cooling runs (10° C min^{-1}). Coupled eutectic growth takes place in the cross-hatched region. The liquidus line of the peritectic region (< 50% WO_3) is drawn tentatively after approximate calculation.

DTA measurements of samples near the eutectic composition often cannot discriminate the solidus from the liquidus peaks during heating. The exact eutectic composition was therefore determined as follows [7, 8]: the relative amounts of the eutectic melts arising from various samples of > 50% WO_3 overall composition increased linearly up to a maximum at the exact eutectic composition, due to the thermodynamic "lever rule" applied on the eutectic tie-line. This linear relationship was reflected by the amounts of the heats-of-fusion as obtained by the evaluation of the peak areas. Increasing the overall WO_3-content of the samples further caused the amounts of the eutectic melts to decrease again to zero at 100% WO_3. (The mutual solubility of solid $NiWO_4$ and WO_3 is < 1% after microprobe measurements.) The statistical evaluation of all eutectic peak areas from heating and cooling runs yielded 73% WO_3 as the eutectic composition. The eutectic temperature was 1245° C.

The peritectic point was established at 55% WO_3 and 1420° C. The melting point of WO_3 at 1420 to 1430° C was in accordance with earlier observations [5]. The liquidus temperatures of overall compositions < 50% WO_3 were mostly above 1600° C and had to be calculated (cf. Section 4.4).

In order to calculate the liquidus lines, the enthalpy of fusion (ΔH_f) of NiO, WO_3 and $NiWO_4$ are required. ΔH_f of NiO and WO_3 are known [16] to amount to 12.1 and 12.6 kcal mol^{-1}, respectively. The enthalpy of the peritectic decomposition of $NiWO_4$ at 1693 K was measured to be ≈ 30 kcal mol^{-1} by the comparison with WO_3 as standard. The peritectic reaction consists theoretically of two steps:

$$NiWO_4(s) \rightarrow NiO(s) + WO_3(s)$$

$$\rightarrow x\,NiO(s) + (1-x)NiO(l) + WO_3(l),$$

where s and l indicate the solid and liquid state, respectively, and x is the amount of solid NiO at the peritectic temperature ($x \approx 0.1$, Fig. 1). The first step corresponds to a solid state reaction at 1693 K and was calculated ($\approx$ 10 kcal mol^{-1}) from the standard enthalpies of formation under consideration of the appropriate heat capacities of the oxides [17–21]. Thus the actual enthalpy of fusion of $NiWO_4$ amounts to ~20 kcal mol^{-1}. X-ray diffraction of the crystalline phases present at room temperature after solidification of melts yields $NiO + NiWO_4$ and $NiWO_4 + WO_3$ in the compositional ranges below and above 50% WO_3, respectively. While NiO and $NiWO_4$ did not show any change of the crystalline state, WO_3 was present as a mixture of its triclinic and monoclinic modifications. The orthorhombic and tetragonal modifications [22, 23] were not observed at room temperature.

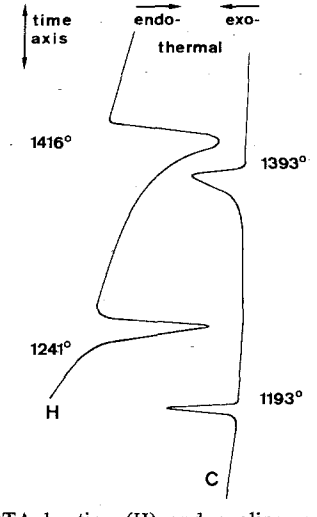

Figure 2 DTA heating (H) and cooling runs (C) of a hyper-eutectic sample (95% WO_3) with noted temperatures of the melting and solidification reactions. The peaks of C are smaller than those of H due to another sensitivity range of the apparatus.

4. Discussion

4.1. Hyper-eutectic phase relations

Fig. 2, H, shows the typical shapes of DTA peaks resulting from melting reactions of hyper-eutectic (> 73% WO_3) samples. The eutectic melting reaction is indicted by a sharp peak. At increasing temperatures, the melting process of the remaining solid WO_3 continues with increasing melting rate according to the flattening of the liquidus line. This gives rise to the concave shape of the "liquidus peak" with its maximum T_p at the liquidus temperature. Samples with nearly eutectic composition have a very small liquidus peak which is mostly overlapped by the strong eutectic one. During cooling, however, both peaks can often be resolved.

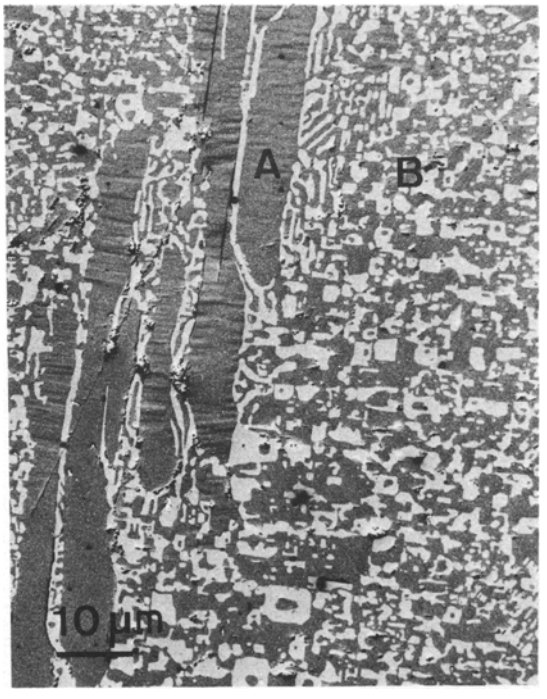

Figure 3 Hyper-eutectic phase morphology (75% WO_3) after rapid solidification (mode A) of the melt. Primary WO_3 crystals (A, dark) are present besides a regular eutectice structure (B) of fibre-like $NiWO_4$ (bright) and WO_3 (dark).

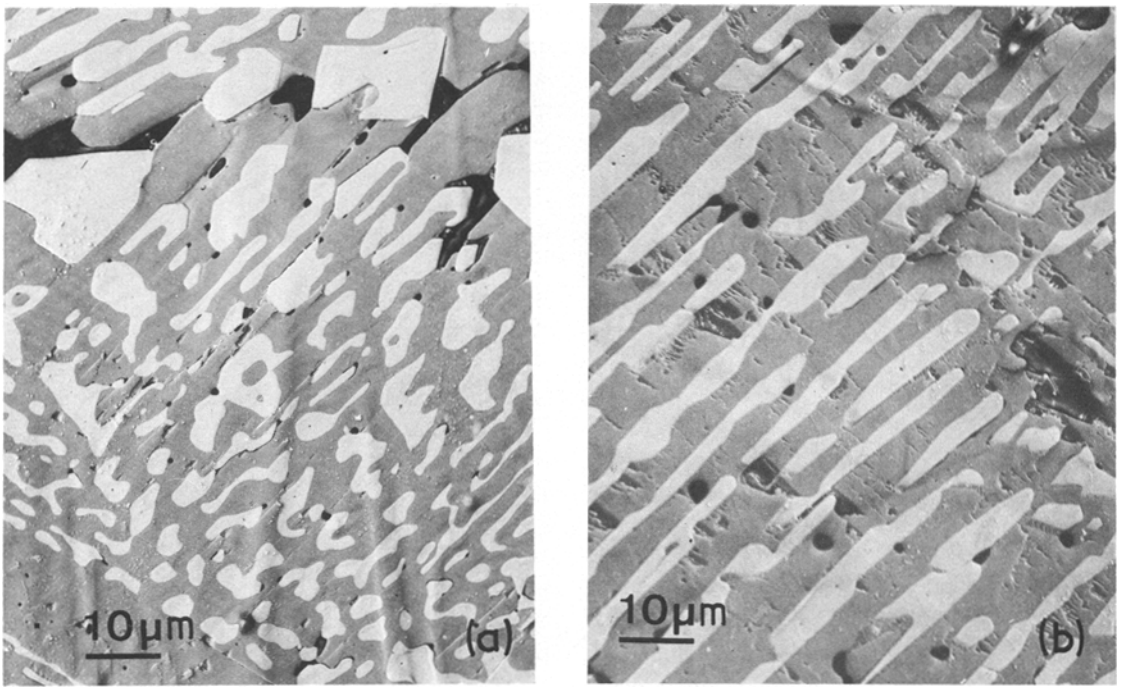

Figure 4 Hyper-eutectic sample (75% WO_3) after slow cooling (mode B) of the melt showing the eutectic morphology in (a) an approximate transversal section and (b) a longitudinal section with respect to the fibre-like $NiWO_4$ (bright) besides the WO_3 constituent (dark).

Liquidus peaks as obtained from cooling runs (Fig. 2, C) are generally not concavely shaped to the same extent as those peaks arising during heating. The reason was not yet investigated exactly, but it can be expected that during cooling the formation of a certain amount of primary crystals is indicated only, while the further continuous crystal growth by consumption of melt is not recorded sensitively enough by DTA.

Undercooling of primary crystallization ($\approx$ 13° C) is relatively low if NiO is present in the melt. Pure WO_3, however, is undercooled 80 to 135° C below its melting point. Increasing undercooling was observed at decreasing cooling rates.

Figs. 3 and 4 reveal the morphology of phases present after rapid (mode A) and slow (mode B) solidification, respectively, of hyper-eutectic melts. Primary WO_3 is surrounded by a regular eutectic structure consisting of $NiWO_4$ as faceted fibres within WO_3. High cooling rates generate smaller dimensions of the several phase regions (Fig. 3) than low cooling rates (Fig. 4).

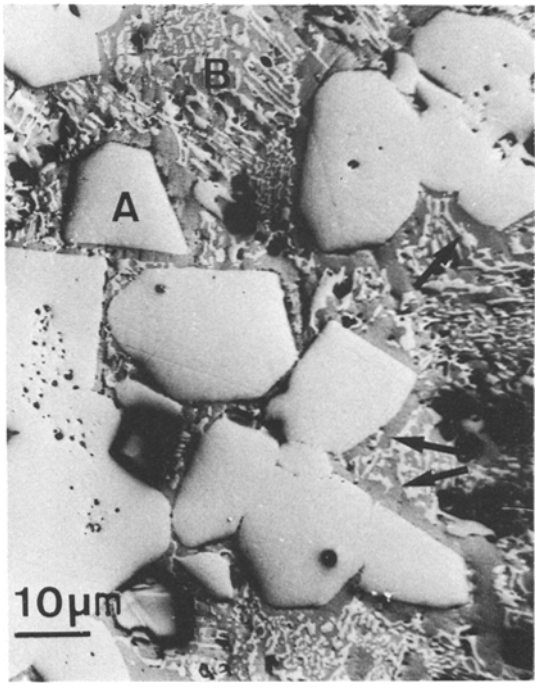

Figure 5 Rapidly solidified (mode A) hypo-eutectic melt (65% WO_3). The primary $NiWO_4$ crystals (A, bright) are surrounded by "haloes" of WO_3 (dark, see arrows) prior to the eutectic coupled growth (B).

4.2. Hypo-eutectic and eutectic phase relations

Appreciable undercooling (90 to 100° C) of the primary crystallization of $NiWO_4$ takes place

from hypo-eutectic melts (50 to 73% WO_3) as observed from DTA cooling runs (Fig. 8, C). Since the remaining eutectic liquid is not undercooled, one can conclude that the primary $NiWO_4$ nucleates the eutectic solidification. On the other side, primary WO_3 from hyper-eutectic melts can obviously not nucleate the eutectic solidification, since the residual eutectic liquid has to be undercooled to just that temperature ($\approx 1200^\circ$ C) at which both metastable liquidus lines intersect each other (cf. Fig. 1). Only at or below the metastable eutectic point ($\approx 70\%$ WO_3) the coupled growth of both eutectic constituents can take place. Fig. 5 shows the morphology of a rapidly cooled (mode A) hypo-eutectic melt. The primary $NiWO_4$ crystals are covered by haloes of WO_3 prior to the formation of the regular eutectic morphology. It follows from this observation that coupled growth is generated only in the compositional region near the metastable hyper-eutectic liquidus line (Fig. 1).

From hypo-eutectic melts $\gtrsim 65\%$ WO_3, primary and eutectic crystallization follow each other so rapidly that they were not resolved by DTA at a cooling rate of 10° C min^{-1}. At a lower cooling rate (2° C min^{-1}) with increased sensitivity of DTA, two large peaks and a small one were observed. The PhEEM micrograph of Fig. 6 shows the formation of a "divorced" eutectic structure: crystallization of $NiWO_4$ and of WO_3 follow each other without "coupled growth" giving rise to the two larger DTA peaks, while the subsequent small one may indicate the solidification of little residual liquid at the boundaries of the larger phase regions.

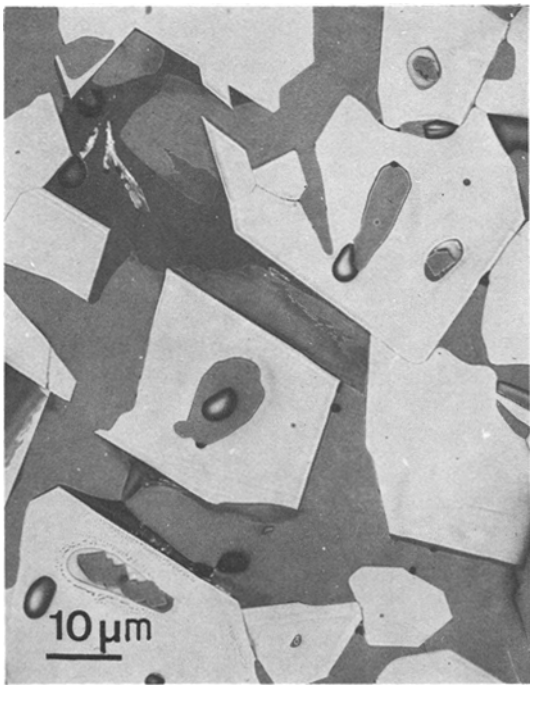

Figure 6 Slowly solidified hypo-eutectic melt (65% WO_3). The "divorced" eutectic structure consists of idiomorphic $NiWO_4$ crystals (bright) which have grown prior to the formation of large regions of WO_3 (dark).

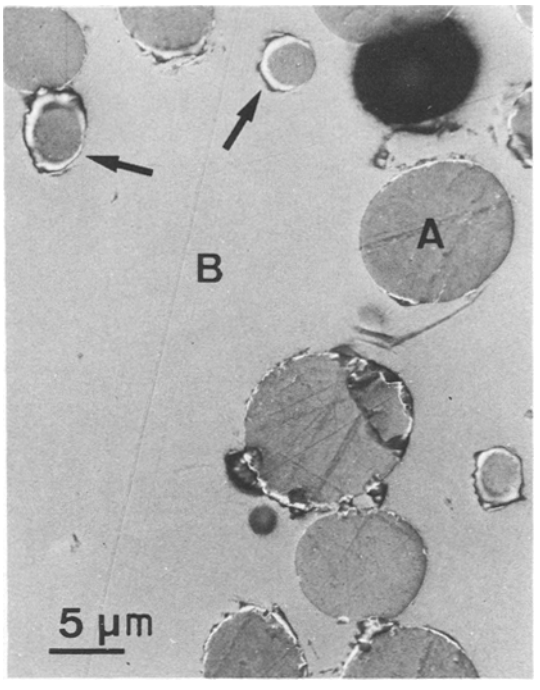

Figure 7 Soldified peritectic melt ($< 50\%$ WO_3) consisting of primary ovoid NiO (A) with peritectic reaction rims (see arrows) besides $NiWO_4$ (B).

4.3. Peritectic phase relations

In the compositional range $< 50\%$ WO_3, primary ovoid NiO is present besides melt above 1420° C. Below this temperature, peritectic solidification occurs without undercooling. The peritectic reaction consists of two steps; at first, the melt reacts with solid NiO to form $NiWO_4$ until the composition of the melt is shifted from 55 to 50% WO_3 (Fig. 1). This gives rise to a reaction rim surrounding the solid primary NiO (Fig. 7). The remaining melt then solidifies as $NiWO_4$. The second step only can be observed by DTA which provides a sufficiently great exothermal enthalpy. During heating of hypo-eutectic samples of 50 to 55% WO_3, the concave liquidus peak is superposed by a larger one (Fig. 8, H) resulting from the highly endothermal peritectic decomposition of $NiWO_4$. Such a thermal effect has also been observed in other phase systems [24].

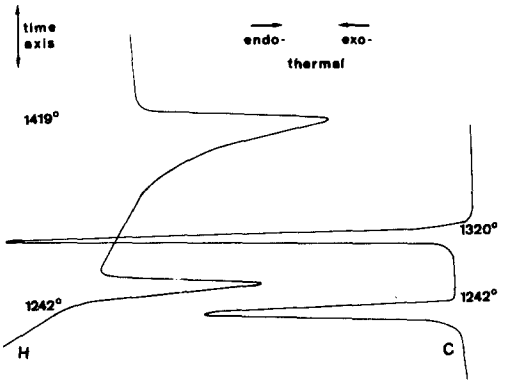

Figure 8 DTA heating (H) and cooling runs (C) of a hypo-eutectic sample (55% WO_3). The concave liquidus peak of H is covered by a strong peak due to the peritectic decomposition of $NiWO_4$. The cooling run C indicates the appreciable undercooling of the crystallization of $NiWO_4$ prior to the eutectic solidification which is not undercooled.

4.4. Discussion of the liquidus lines

Liquidus lines can be calculated approximately from thermodynamic relations [25]. The equation

$$\ln\left(\frac{X_A^s}{X_A^l}\right) = \frac{\Delta H_{f,A}}{RT_{f,A}}\,\frac{\Delta T}{T}$$

describes the lowering of the melting point $T_{f,A}$ of the compound A with reference to the enthalpy of fusion $\Delta H_{f,A}$ and to the molar fraction of A in the coexisting solid X_A^s and liquid X_A^l at the actual temperature T. ΔT means the difference $T_{f,A} - T$, and R is the gas constant. This equation was earlier applied successfully to complex oxide systems [26] although it implies the "ideal" mixing behaviour of the liquid melt. By application of this equation using $X^s(NiO) = 1$ and $X^l(NiO) = 0.45$ at the peritectic temperature $T = 1693\,K$, $\Delta H_f(NiO) = 11\,kcal\,mol^{-1}$ is obtained, which is in good agreement with the known value [16] of $12.1\,kcal\,mol^{-1}$. On the other hand, $X^l(NiO)$ can be calculated at various temperatures and yields the liquidus line of the peritectic region (< 55% WO_3, Fig. 1).

In the same way, $\Delta H_f(NiWO_4) = 17\,kcal\,mol^{-1}$ was obtained using $X^s(NiWO_4) = 1$ and $X^l(NiWO_4) = 0.54$ at the eutectic temperature $T = 1518\,K$. This value is again in reasonable agreement with the experimental amount of about $20\,kcal\,mol^{-1}$ (Section 3). The experimental hypo-eutectic liquidus line can therefore also be confirmed roughly by calculation.

The experimental liquidus line of the hyper-eutectic side of the diagram, however, can be confirmed by calculation only if ΔH_f is assumed to be about $21.5\,kcal\,mol^{-1}$ instead of the $12.6\,kcal\,mol^{-1}$ [16] of the pure compound. Consequently, ΔH_f in the equation above has to be supplemented by a positive enthalpy of mixing ΔH_m of the liquid mixture $WO_3 + NiO$ according to the "regular solution model" [27].

The positive enthalpy of mixing of the WO_3-rich liquids indicates the tendency to immiscibility and may be discussed in some analogy to the better known silicate systems [28, 29]. The solid WO_3 consists of WO_6-octahedra linked by all oxygens at the corners. This structure is partially broken in the melt, but polyhedra chains or branches are assumed to be still present. Similar to SiO_2, molten WO_3 tends therefore to supercooling as observed in this work. By rapid quenching of the melt, WO_3 even appears in a glass-like state [30].

Additional oxides in the melt give rise to a separation of the polymerized WO_6-polyhedra due to the presence of exceeding oxygen. The equation $O^0 + O^{2-} \rightleftharpoons 2O^-$ then describes the formation of singly bounded oxygen (O^-) in isolated WO_6-polyhedra from additional free oxygen ions (O^{2-}) and decreasing amounts of doubly bounded oxygen (O^0) in polymers. This process of depolymerization is particularly generated by additional alkaline oxides where the cation has only a small field strength $F = Z/a^2$, where Z is the charge and a is the radius of the cation, respectively. The proportionality

$$F \sim \frac{\Delta H}{RT^2} \approx \frac{X_{BO}^l}{\Delta T}$$

(where X_{BO}^l is the molar fraction of the additional oxide in the melt) was found as an empirical rule in SiO_2- and WO_3-rich melts [31]. Small values of F give rise to lowering of ΔH due to a negative enthalpy of mixing of the liquid melt. With increasing bond strength between the additional cation and oxygen due to a larger field strength F, the concentration of the actual O^{2-} decreases, and hence the depolymerization of WO_3 in the melt is hampered. This gives rise to the formation of separated "clusters" of both oxides, and ΔH_m is increased. In the present case of additional NiO with relatively large F, the positive ΔH_m generates metastable liquid immiscibility which explains the strongly reduced undercooling of NiO-containing

hyper-eutectic melts in comparison with the pure WO_3. In other words, the metastable hyper-eutectic liquidus line represents the solvus of the metastable liquid immiscibility region.

5. Conclusions

The phase diagram of the system NiO–WO_3 (Fig. 1) contains one compound, $NiWO_4$, which melts incongruently by peritectic decomposition (1420° C) and forms a eutectic with WO_3 at 73 mol % WO_3 and 1245° C.

The stable phase relations were established by DTA heating runs (10° C min^{-1}) while the cooling runs (10° C min^{-1}) revealed some characteristic undercooling effects: on the hypo-eutectic side, the crystallization of primary $NiWO_4$ is undercooled to about 90 to 95° C. The subsequent eutectic solidification is nucleated by the presence of primary $NiWO_4$, whereas primary WO_3 on the hyper-eutectic side cannot nucleate the eutectic growth. The normal eutectic structure consists of faceted $NiWO_4$ fibres within WO_3. It is generated by slow or rapid cooling of hyper-eutectic melts or by rapid cooling of hypo-eutectic melts. Slow cooling of hypo-eutectic melts, however, generates a "divorced" eutectic morphology.

The melt of pure WO_3 is undercooled to about 80 to 130° C, whereas primary formation of WO_3 from hyper-eutectic melts is undercooled only slightly ($\approx$ 13° C). This different behaviour can be explained by the effect of metastable liquid immiscibility of hyper-eutectic melts due to a strongly positive enthalpy of mixing which is caused by the high field strength of the Ni^{2+} cation and the partial polymerizationof WO_3 in the melt.

Acknowledgements

We thank Professor H. R. Oswald for his stimulating interest in this work and Miss E. Grauer-Carstensen for technical assistance in PhEEM. The financial support by the Swiss Commission for the Encouragement of Scientific Research (Project Number 791.1) is gratefully acknowledged.

References

1. L. LUKE, Y. CHANG, M. G. SCROGER and B. PHILLIPS, *J. Amer. Ceram. Soc.* **49** (1966) 385.
2. B. PHILLIPS, L. LUKE and M. G. SCROGER, *Trans. Met. Soc. AIME* **233** (1965) 1220.
3. J. T. RICHARDSON and W. O. MILLIGAN, *Phys. Rev.* **102** (1956) 1289.
4. J. OISHI, M. AWANO and T. MOCHIZUKI, *J. Phys. Soc. Japan* **11** (1956) 311.
5. B. PHILLIPS, in 'Refractory materials' edited by M. Alper, part IV (Academic Press, New York, 1971) p. 109.
6. S. C. SOUTHARD and A. E. MOORE, *J. Amer. Chem. Soc.* **64** (1942) 1769 .
7. A. GAEUMANN, *Chimia* **20** (1966) 82.
8. A. GAEUMANN and J. OSWALD, *ibid* **21** (1967) 421.
9. G. WILLMANN, *Z. Anal. Chem.* **269** (1974) 257.
10. R. MELLING, R. W. WILLBURN and R. M. McINTOSH, *Anal. Chem.* **41** (1969) 1275.
11. L. G. BERG and V. P. EGUNOV, *J. Therm. Anal.* **2** (1970) 53.
12. J. SESTAK and G. BERGGREN, *Chem. listy* **64** (1970) 695.
13. B. J. KOLM and J. L. HOLM, *Thermochim. Acta.* **5** (1973) 273.
14. L. WEGMANN, *Microscopy* **96** (1972) 1.
15. L. WEBER and H. R. OSWALD, *J. Mater. Sci.* **10** (1975) 973.
16. A. GLASSNER, *Argonne Nat. Lab. (ANL)* **5107** (1953).
17. E. G. KING, *J. Amer. Chem. Soc.* **79** (1957) 2399.
18. E. G. KING and A. H. CHRISTIANSEN, *ibid* **80** (1958) 1800.
19. E. G. KING and A. U. CHRISTIANSEN, *J. Phys. Chem.* **62** (1958) 499.
20. K. K. KELLY, "Contributions to the data on theoretical metallurgy" Vol. X, Washington (1932–1949).
21. L. A. ZHARKOVA and T. N. REZUKHINA, *Zh. Fiz. Khim.* **32** (1958) 2233.
22. S. IIJIMA, *J. Sol. State Chem.* **14** (1975) 52.
23. A. MAGNELI, *Acta. Chem. Scand.* **11** (1957) 28.
24. D. E. ETTER, P. A. TUCKER and L. J. WITTENBERG, Proceedings of the 2nd International Conference on Thermal Analysis **2** (1968) 829.
25. P. GORDON "Principles of phase diagrams in materials systems", (McGraw–Hill, New York, 1968) p. 77.
26. S. A. SUVOROV and V. K. NOVIKOV, *Inorg. Materials* **7** (1971) 246.
27. J. H. HILDERBRAND, J. M. PRAUSNITZ and R. L. SCOTT, "Regular and related solutions" (Van Nostrand Reinhold, New York, 1970).
28. P. C. HESS, *Geochim. Cosmochim. Acta.* **35** (1971) 289.
29. M. L. KAPOOR, G. M. MEHROTRA and M. G. FORHBERG, *Arch. Eisenhuettenw.* **45** (1974) 663.
30. P. T. SARGEANT and R. ROY, *J. Amer. Ceram. Soc.* **50** (1967) 500.
31. L. STOCH, *ibid* **51** (1968) 419.

Received 10 January and accepted 18 February 1977.